



Starch-graft-polyacrylamide copolymer /Fe₃O₄ /graphene oxide nanocomposite: synthesis, characterization, and application as a low-cost adsorbent for Ni (II) from aqueous solutions

Sh. H. Hegazy¹ · S. K. Mohamed¹

Received: 15 June 2020 / Accepted: 3 September 2020 / Published online: 15 January 2021
© The Polymer Society, Taipei 2021

Abstract

Starch-g-polyacrylamide copolymer and its nanocomposite with Fe₃O₄ and graphene oxide have been successfully synthesized. The synthesized samples were characterized using FTIR, XRD, SEM, HRTEM, and VSM. The factors that affect the adsorption efficiency of samples for Ni(II) ions from aqueous solutions as pH, initial Ni(II) ions concentration, contact time and temperature have been examined. The maximum adsorption capacities achieved by the synthesized samples were 195 mg g⁻¹ and 290 mg g⁻¹ for starch-g-polyacrylamide copolymer and its starch-g-polyacrylamide/ Fe₃O₄/ graphene oxide nanocomposite respectively. Kinetic studies showed that the adsorption was well described by the pseudo-second-order model and the equilibrium adsorption data fitted Freundlich model. Thermodynamic studies showed that the adsorption capacity increases as temperature increase up to 313 K but higher temperatures result in dissolution of starch. Results showed that the adsorption process is spontaneous, endothermic in nature and leads to a greater entropy.

Keywords Adsorption · Kinetics · Thermodynamics · Starch · Composite

Introduction

Industrial activities generate a huge amount of waste including toxic and carcinogenic inorganic pollutants as heavy metals and organic pollutants as dyes and pesticides. When heavy metal ions exceed definite limits in aqueous systems, it is considered as toxic and carcinogenic materials. Despite organic wastes, heavy metals as nickel, lead, copper, iron, cobalt, molybdenum, manganese, etc. are not biodegradable and end up as accumulated pollutants in the environment [1]. In addition to the industrial wastewater contaminated with heavy metal ions, heavy metals naturally exist in the earth's crust and by the action of acidic rains, it may dissolve and release into rivers, streams, and groundwater. According to the World Health Organization (WHO), the nickel ions concentration should not exceed 0.02 mg L⁻¹ since below this limits Ni (II) ion is required for some metabolic reactions.

However, a higher concentration of Ni (II) ions inhibits the activity of enzymes and causes damages in the lungs, kidney and skin [2]. Among the various physicochemical techniques for heavy metals removal from aqueous media, adsorption is considered as a powerful technique because it is a fast, inexpensive and easy method. Many researchers studied the development of low cost biodegradable adsorbents for heavy metals as sesame straw biochar [3], rice bran [4], activated carbon [5], Coconut leaves [6] and sweet lime peel [7]. Natural polymers adsorbents are good options for heavy metals because they are abundant, nontoxic, biocompatible, biodegradable, eco-friendly and have plenty of adjustable functional groups. Chitosan [8–10], alginate [11], starch [12–14] and gelatin [15] were examined as adsorbents for heavy metals. Modification of natural polymers by grafting with monomers/polymers enhances the adsorption efficiency of the polymer by introducing additional functional groups to the polymeric matrix. Also, attempts to improve the adsorption efficiency of natural polymers by impregnation of nanoparticles of inorganic materials as magnetite (Fe₃O₄) or/and carbonaceous compounds have been extensively studied. Iron oxide is abundant, cheap, and non-toxic, has a high surface area and high efficiency for adsorption of heavy metals [16]. To the best of our knowledge, only few

✉ S. K. Mohamed
sahar.kamal@science.helwan.edu.eg;
sahar_km2@yahoo.com

¹ Chemistry Department, Faculty of Science, Helwan University, Ain Helwan, Cairo 11795, Egypt

researches focused on using starch or starch composites for removal of heavy metals as polyacrylonitrile grafted cassava starch hydrogel [17], crosslinked starch [18, 19], modified starch/magnetite nanocomposite [20].

In this article, starch-g-polyacrylamide and its composite with magnetite (Fe_3O_4) nanoparticles and graphene oxide (GO) have been synthesized. The grafting crosslinking polymerization reaction of acrylamide with starch was carried out in the presence of GO and Fe_3O_4 nanoparticles. The synthesized samples were examined by FTIR, XRD, SEM, TEM and VSM. The kinetics, isotherms and thermodynamic studies of the adsorption of the synthesized samples for Ni (II) ions have been studied. The adsorption efficiency of starch-g-polyacrylamide for removal of Ni (II) ions was compared to that of starch-g-polyacrylamide copolymer/ Fe_3O_4 /GO nanocomposite.

Experimental

Materials

Starch and ferric chloride hexahydrate ($\text{FeCl}_3 \cdot 6\text{H}_2\text{O}$) were obtained from (Alpha Chemika, India), N,N'-methylenebisacrylamide (MBA, Merck, Germany), Acrylamide (AAM) and ferrous chloride tetrahydrate ($\text{FeCl}_2 \cdot 4\text{H}_2\text{O}$) (WIN-LAB, India), Ceric ammonium nitrate (CAN) (Alfa Aesar, Germany), graphite fine powder extra pure (Loba Chemie, India). Nickel nitrate hexahydrate $\text{Ni}(\text{NO}_3)_2 \cdot 6\text{H}_2\text{O}$ (Sigma-Aldrich). All other reagents were analytical reagent grade and were used as received.

Synthesis

Synthesis of magnetite (Fe_3O_4)

Magnetite (Fe_3O_4) was prepared by co-precipitation according to the modified Massart method [21]. In this method, a mixture of $\text{FeCl}_3 \cdot 6\text{H}_2\text{O}$ (3.03 g) and $\text{FeCl}_2 \cdot 4\text{H}_2\text{O}$ (1.13 g) was dissolved in distilled water (150 ml) at 60 °C under stirring. Ammonia solution was added to the obtained yellow solution slowly during stirring till the mixture's pH is 10.0. The reaction mixture was purged by N_2 gas during the reaction. After 1 h of vigorous stirring, the obtained black precipitate was filtered, rinsed several times by deionized water and ethanol and then dried in an oven at 60 °C.

Synthesis of graphene oxide (GO)

Graphene oxide (GO) was prepared by the modified Hummers method [22]. Briefly, graphite (5 g) was mixed with H_2SO_4 98% (230 ml) then NaNO_3 (5 g) was added. After 30 min, KMnO_4 (30 g) was gently added and mixed

thoroughly and later deionized water (300 ml) was added. The whole reaction was carried out in an ice bath under continuous stirring to control the rapid rise in reaction temperature. The reaction mixture was stirred till cooled down then H_2O_2 (30%) was added. The mixture was centrifuged to and the obtained precipitate was washed several times with 5% HCl followed by deionized water. The obtained GO was dried at 50 °C, and then crushed using a mortar.

Synthesis of starch-g-polyacrylamide copolymer and its nanocomposite with Fe_3O_4 and GO

Starch-g-polyacrylamide copolymer was prepared by dispersing 3 g of starch in 75 ml distilled water then gelatinizing it at 100 °C for 15 min. In a test tube, 0.3 g (CAN) was dissolved in 1 M HNO_3 then added to the gelatinized starch. The reaction mixture was stirred at 60 °C under nitrogen atmosphere for 15 min to allow the free radicals formation. A solution of AAM (3 g) and MBA (0.07 g) was added to the reaction mixture and allowed to react for 2 h. After that, a solution of NaOH (4.1 g dissolved in 75 ml distilled water) was added to the reaction mixture and stirred for 2 h at 90 °C. The obtained grafted starch was filtered, washed several times by distilled water and dried in an oven at 60 °C and this sample was labeled as gSt. To prepare starch-g-polyacrylamide/ Fe_3O_4 /GO nanocomposite the same procedure was used where Fe_3O_4 (0.15 g) and GO (0.15 g) were dispersed in 300 ml distilled water and this dispersion was sonicated using a tip sonicator for 1 h to get a homogeneous dispersion. This dispersion was added immediately after sonication to the starch dispersion after the initiation step. The obtained polymer nanocomposite was labeled as gSt/ Fe_3O_4 /GO.

Characterization

Fourier transform infrared (FTIR) spectra were recorded on a FTIR spectroscopy (FT-IR-6100 Jasco, Japan), using KBr pellets in the range of 4000–400 cm^{-1} at room temperature with spectral resolution 4 cm^{-1} . X-Ray diffraction analysis was carried out using X-Ray Diffractometer (X'Pert Pro, PANalytical, Netherlands) using Cu K α radiation ($\lambda = 0.15406$ nm) in the 2θ range of 4° to 70°. The morphology of the samples was investigated using Field Emission Scanning Electron Microscope (FE-SEM) (Quanta FEG 250, NL). The samples were coated with gold before FE-SEM testing. High Resolution Transmission Electron Microscope (HRTEM) analysis was carried out on a JEOL JEM-2100 Plus (USA) Transmission

Electron Microscope. In addition, the magnetic properties of the synthesized Fe_3O_4 and $\text{gSt}/\text{Fe}_3\text{O}_4/\text{GO}$ were examined using a vibrating sample magnetometer (VSM, CRMDI) at room temperature.

Adsorption experiments

In each adsorption experiment, 0.1 g of the adsorbent was immersed in 50 ml of Ni (II) aqueous solution with a definite initial concentration, temperature and initial pH using HCl 0.1 M and NaOH 0.1 M solutions. The concentration of the Ni (II) solution was measured on atomic absorption spectrometer AAnalyst 400–PerkinElmer. The adsorption percentage (%E) and the amount of adsorbed Ni (II) ions, q_e (mg g^{-1}), were calculated as follows:

$$\%E = \frac{(C_o - C_e)}{C_o} * 100 \quad (1)$$

$$q_e = (C_o - C_e) \frac{V}{m} (\text{mg g}^{-1}) \quad (2)$$

where C_o and C_e are the initial and equilibrium concentration of Ni(II) ions in the solution (mg L^{-1}), respectively. V is the volume of the solution (L) and m is the mass of the adsorbent in grams.

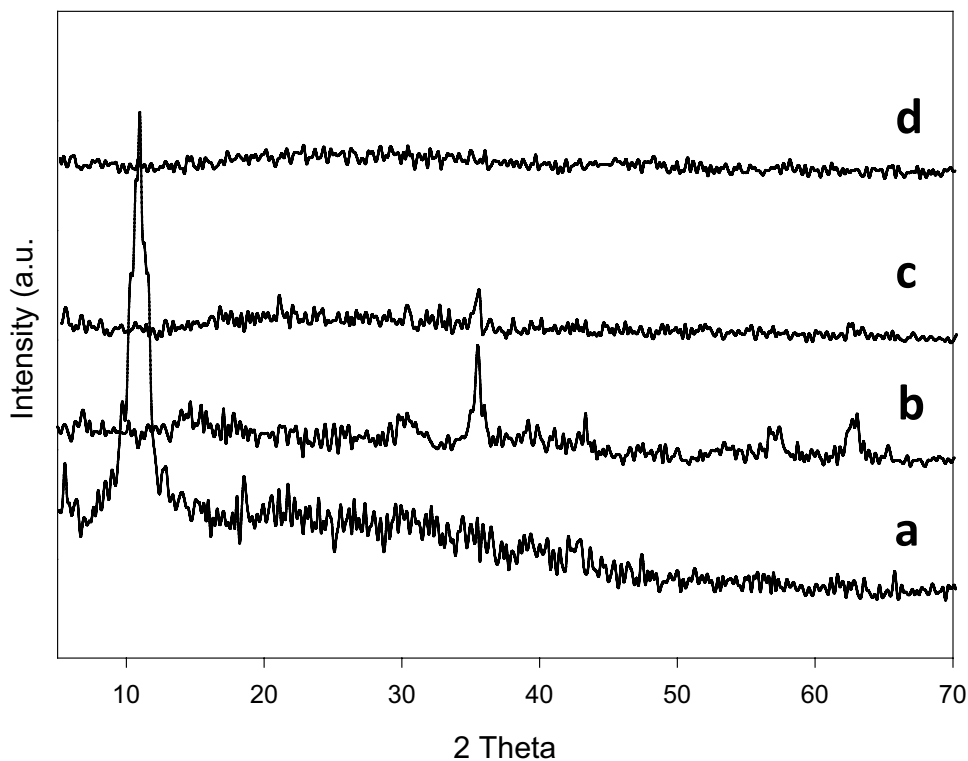
Results and discussion

Characterization

XRD

The crystallinity and other structural properties of the investigated samples were examined by XRD and presented in Fig. 1. The XRD pattern of Fe_3O_4 showed characteristic peaks at 2 theta values of 30.3, 35.5, 43.2, 53.3, 57.4 and 62.7 corresponding to (220), (311), (400), (422), (511), and (440) planes, respectively (JCPDS file PDF no.65–3107) [23]. XRD pattern of GO showed a strong sharp diffraction peak at 2θ value of 10.8 which was ascribed to (002) plan with the basal spacing of 0.818 nm [24]. The absence of diffraction peaks in the XRD pattern of gSt indicates the amorphous structure of the grafted polymer. The XRD pattern of $\text{gSt}/\text{Fe}_3\text{O}_4/\text{GO}$ nanocomposite showed small sharp peaks around 2-theta values of 35 and 62 which revealed to Fe_3O_4 crystals. However, the other characteristic diffraction peaks were not obvious probably due to the small content of Fe_3O_4 in the nanocomposite which results in low intensity for these diffraction peaks. In addition, the sharp characteristic peak of GO did not appear in $\text{gSt}/\text{Fe}_3\text{O}_4/\text{GO}$ nanocomposite which attributed to either the complete exfoliation of GO sheets in the polymer or the partial exfoliation leaving a small amount of crystalline GO [25].

Fig. 1 XRD patterns of synthesized samples (a) GO; (b) Fe_3O_4 ; (c) $\text{gSt}/\text{Fe}_3\text{O}_4/\text{GO}$ nanocomposite and (d) gSt



FT-IR

FT-IR spectra of both synthesized samples are shown in Fig. 2. The characteristic peak around 3440 cm^{-1} corresponds to stretching vibrations of O–H and N–H bonds where the intensity of this peak was greater in the case of gSt/ Fe_3O_4 / GO nanocomposite due to the extra hydroxyl groups from GO sheets. The peaks at 2860 and 2930 cm^{-1} belong to the stretching vibrations of aliphatic C–H [26]. The peak at 1630 cm^{-1} is attributed to the stretching vibration of C=O of acrylamide –CONH₂ group [27]. The observed peak at 1050 for both samples belongs to C–O, however, this peak was broadened in the case of gSt/ Fe_3O_4 / GO nanocomposite due to the presence of GO [28]. In the case of gSt/ Fe_3O_4 / GO nanocomposite, The additional peaks at 1450 cm^{-1} (aromatic C=C), 1550 cm^{-1} (asymmetric COO) and the shoulder at 1410 cm^{-1} (symmetric COO) confirm the incorporation of GO in the nanocomposite sample [29]. The peaks around 660 cm^{-1} in the case of gSt/ Fe_3O_4 / GO nanocomposite belongs to stretching vibration of Fe–O bond which confirms the presence of Fe_3O_4 nanoparticles in the polymeric matrix [27].

FE-SEM

Figure 3 shows the SEM micrographs of gSt/ Fe_3O_4 / GO. As shown in Fig. 3a the sample surface exhibits homogeneous distribution for Fe_3O_4 aggregates (light color) where

the image shows a GO sheet within the polymeric matrix that is covered homogeneously with Fe_3O_4 aggregates. Figure 3b showed large clusters of Fe_3O_4 aggregates on the polymeric surface. These results indicated that the magnetite is homogeneously distributed on the polymeric surface as aggregates; however, some areas on the surface are heavily covered with aggregated Fe_3O_4 .

HRTEM

Figure 4 illustrates the HRTEM image for gSt/ Fe_3O_4 / GO nanocomposite. The dark areas represent GO sheets where the dark spheres that are distributed on its surface are Fe_3O_4 nanoparticles while the light background represents the polymeric matrix. Images show that the Fe_3O_4 nanoparticles have diameters ranging from 7 to 9 nm. It was observed that Fe_3O_4 nanoparticles mainly decorate the GO sheets which suggest an interaction between Fe_3O_4 and GO through Fe–O–C bonds as mentioned previously by other authors [30]. This was attributed to the sample preparation method at which Fe_3O_4 was dispersed in GO suspension and the mixture was sonicated for enough time to interact with each other before addition to the polymer.

VSM

The magnetization curve of Fe_3O_4 and gSt/ Fe_3O_4 / GO nanocomposite are shown in Fig. 5. The saturation magnetization

Fig. 2 FTIR spectra of gSt and gSt/ Fe_3O_4 / GO nanocomposite

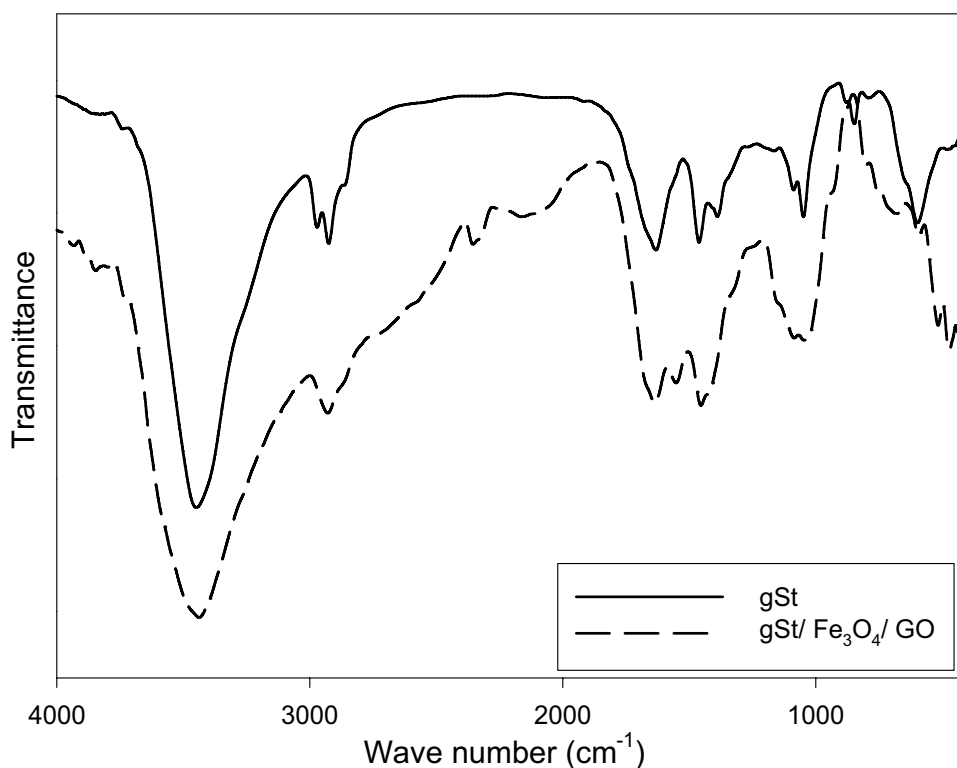


Fig. 3 SEM micrographs of St/
Fe₃O₄/GO nanocomposite

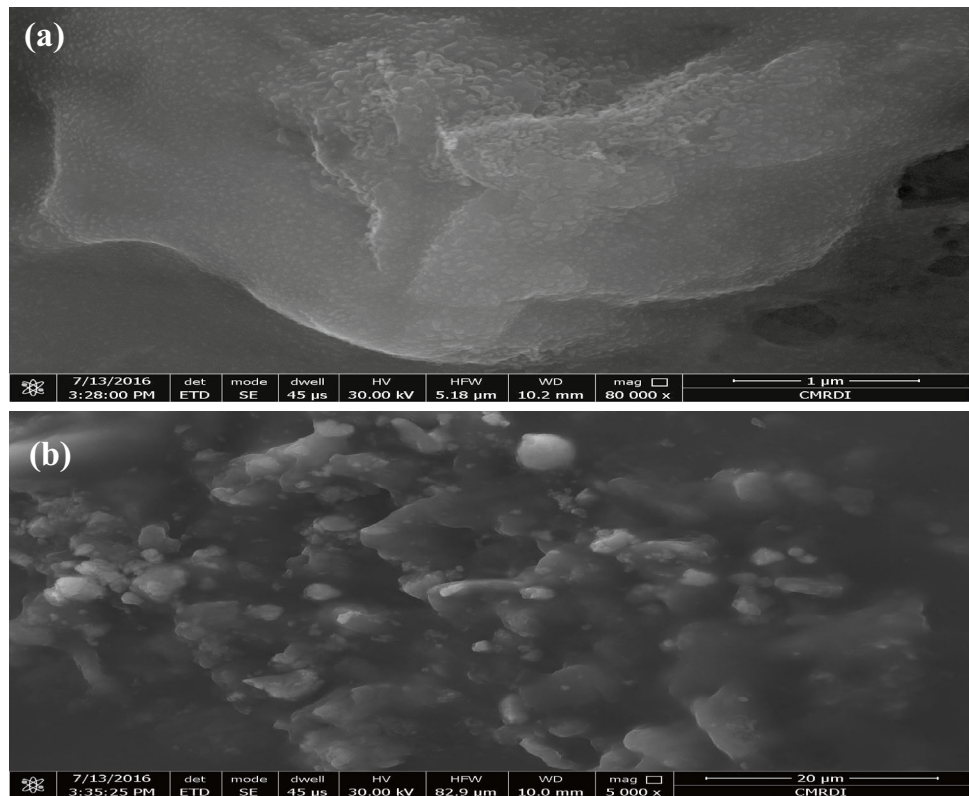
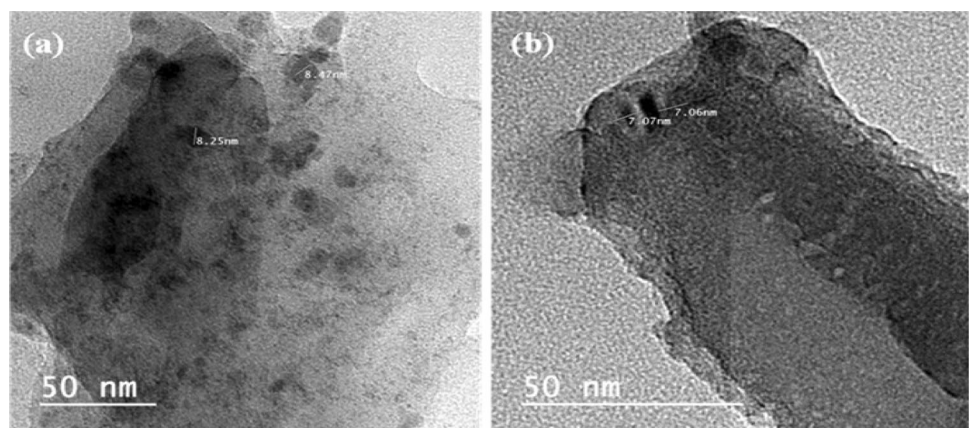


Fig. 4 HRTEM image of gSt/
Fe₃O₄/GO nanocomposite
sample



was 98.56 and 0.95 emu g⁻¹ for Fe₃O₄ and gSt/Fe₃O₄/GO respectively. In addition to the coverage of Fe₃O₄ nanoparticles by the polymer, the low content of Fe₃O₄ leads to a negligible saturation magnetization value for the nanocomposite. The saturation magnetization value is measured per g of materials then its value is proportional to the content of Fe₃O₄ per gram of nanocomposite [31].

Adsorption studies

Adsorption and pH dependence

The pH of the adsorbate solution deeply affects the adsorption capacity because it affects the charge of the adsorbent surface and the degree of ionization of the functional groups

Fig. 5 VSM patterns of the synthesized (a) Fe_3O_4 and (b) gSt/ Fe_3O_4 /GO nanocomposite

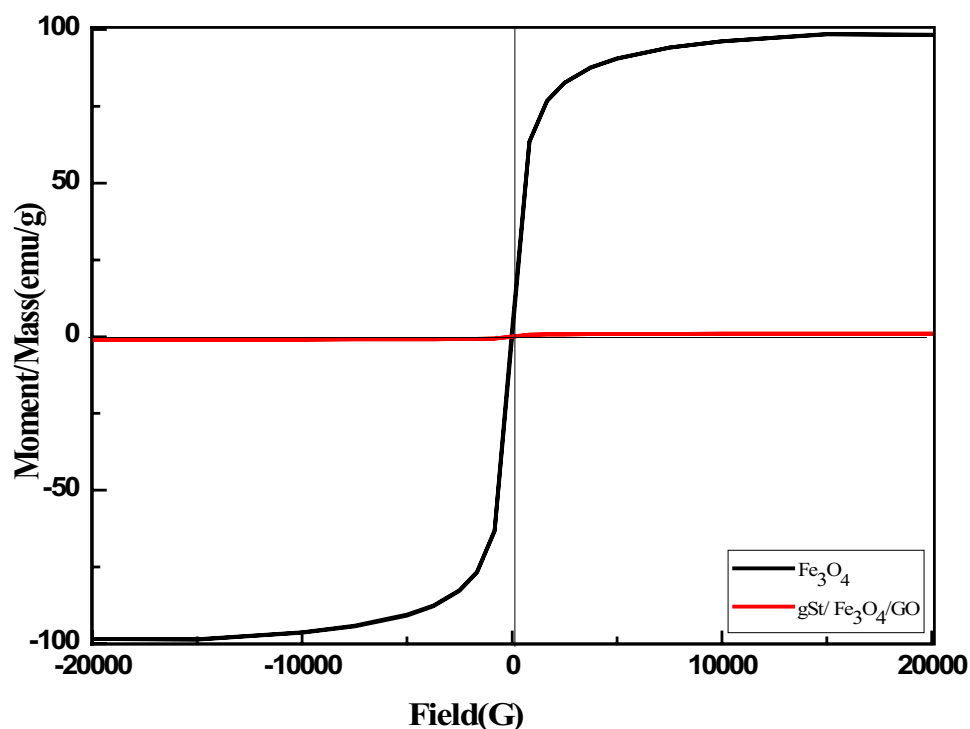
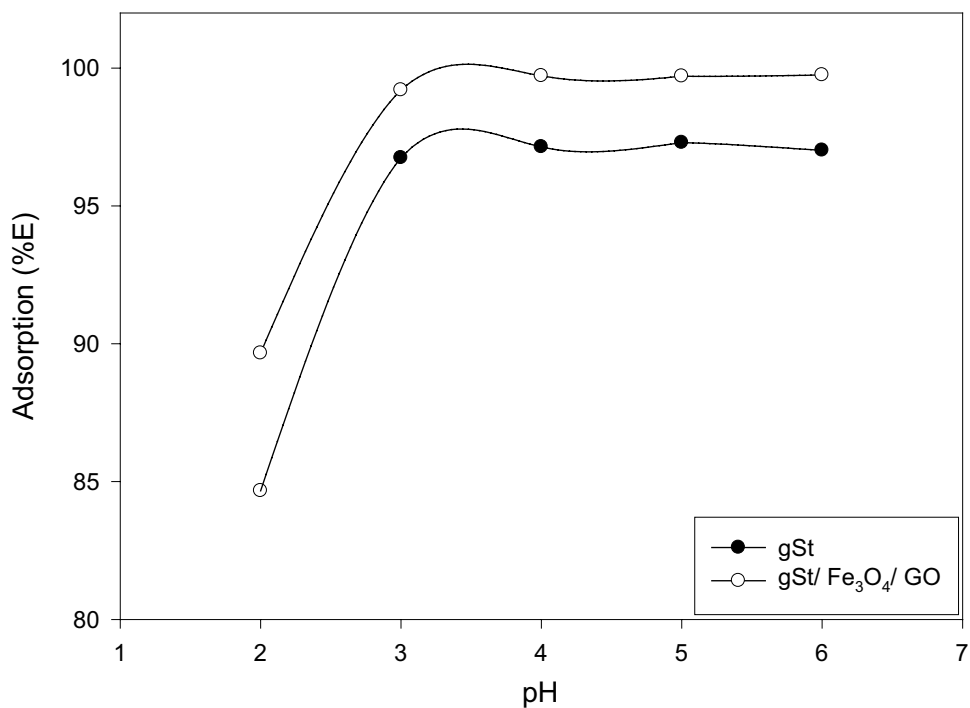


Fig. 6 Effect of pH on Ni (II) adsorption on synthesized samples



on the adsorbent. To investigate the effect of initial pH of Ni (II) ions solution on the adsorption (%E) of the synthesized samples, 0.1 g of each adsorbent was immersed in 50 ml of Ni (II) ions solution (20 mg L^{-1}) with initial pH 2, 3, 4, 5, and 6 for 24 h at 20°C with continuous shaking. Figure 6 shows how the adsorption (%E) is changed with the initial

pH of Ni (II) ions solution. As shown, both samples showed the lowest adsorption (%E) at pH 2 which was attributed to the protonation of NH_2 of polyacrylamide side chains those results in the repulsion of the cationic species Ni (II) ions. In addition, in strong acidic mediums, H^+ ions present in excess in the solution and hence compete the Ni (II) ions. At all

studied pH values, gSt/ Fe₃O₄/ GO nanocomposite showed greater adsorption (%E) than gSt. In the case of gSt/ Fe₃O₄/ GO nanocomposite, the presence of GO sheets with plenty of OH groups provides extra hydrophilicity that increases the degree of swelling. In addition, the presence of Fe₃O₄ restricts the H bonding which also enhances the swelling and hence the adsorption efficiency [32].

Effect of contact time

Figure 7 shows the change of adsorption (%E) of the synthesized samples with the contact time. The maximum adsorption capacity (q_e) attained after 24 h was detected experimentally as 9.028 and 9.5 mg g⁻¹ for gSt and gSt/ Fe₃O₄/ GO respectively. During the first 30 min of the adsorption reaction, the adsorption (% E) reached 61.2, 64.5% for gSt and gSt/ Fe₃O₄/ GO respectively which was attributed to the availability of most of the active sites on the adsorbent surface. As the adsorption reaction precedes, the available active sites on the adsorbent decrease, so the rate of adsorption process slows down.

Effect of initial concentration

To investigate the saturation capacity of the adsorbent, adsorption experiments were carried out using Ni (II) solutions of different initial concentrations. In each experiment, 0.1 g adsorbent was soaked in a Ni (II) solution of concentration range (20—500 mg L⁻¹), pH 5 at 20 °C for 24 h with

shaking. The obtained equilibrium adsorption capacity (q_e) is plotted versus the different initial Ni (II) concentration and presented in Fig. 8. It is obvious that as the initial concentration of Ni (II) ions increased from 20 to 500 mg L⁻¹, q_e increased from 9.08 to 195 mg g⁻¹ for gSt and 290 mg g⁻¹ for gSt/ Fe₃O₄/ GO. Up to initial concentration 500 mg L⁻¹, the samples did not show saturation as increasing the initial concentration of the Ni (II) ions enhances the mass transfer from the solution to the adsorbent as a result of the concentration gradient.

Adsorption kinetics and mechanism

The kinetic studies for adsorption of any pollutant from aqueous solutions on/onto solid adsorbent indicate the adsorption reaction pathway. To investigate the kinetics of the adsorption reaction, the well-known pseudo-first-order and pseudo-second-order models were used to interpret the experimental results. Also, the intra-particle diffusion model was used to analyze the experimental results to explore the adsorption mechanism.

Pseudo-first-order model

The pseudo-first-order model has been extensively used to study the adsorption in liquid–solid systems based on the sorption capacity of solids. The linear form of this model is expressed as:

Fig. 7 Effect of contact time on adsorption (% E) [adsorbent dose, 0.1 g; Ni (II) solution concentration, 20 mg L⁻¹; initial pH, 5.0 and 20 °C for 24 h]

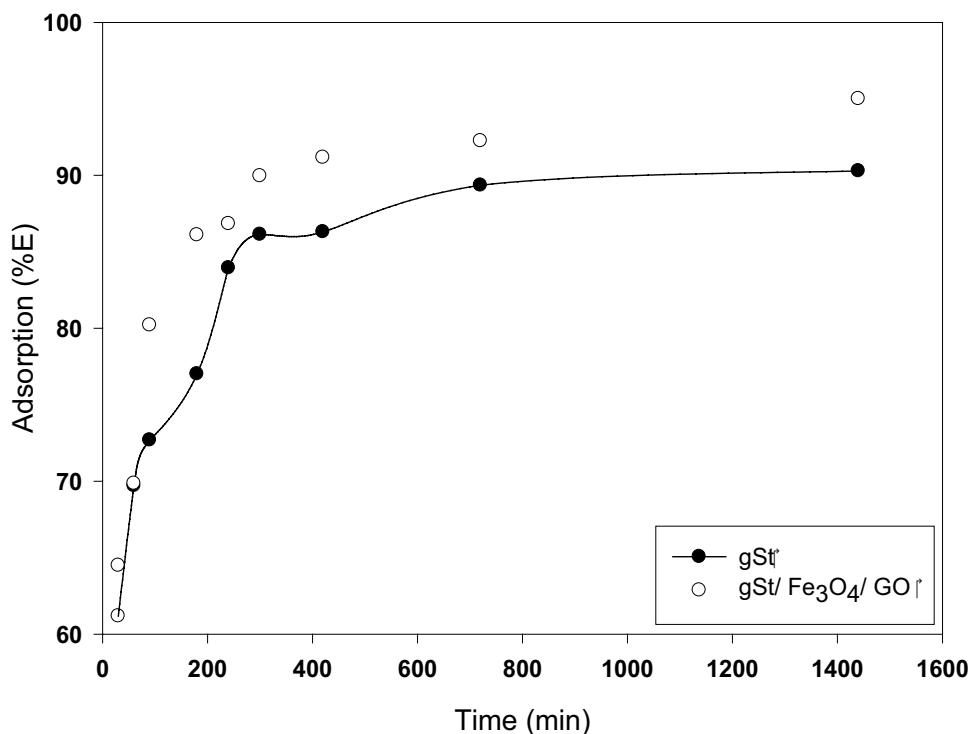
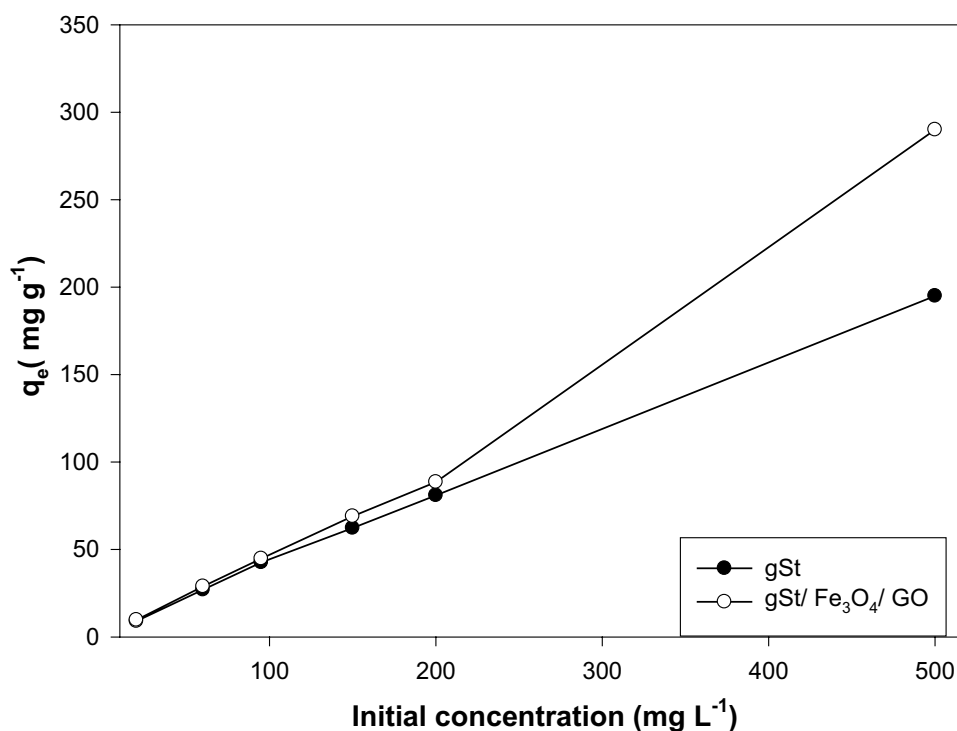


Fig. 8 Effect of initial Ni (II) concentration on the adsorption capacity of samples [adsorbent dose, 0.1 g at pH 5.0 and 20 °C for 24 h]



$$\log(q_e - q_t) = \log q_e - \left(\frac{k_1 t}{2.303}\right) \quad (3)$$

where q_t is the amount of pollutant adsorbed (mg g^{-1}) at any time t and q_e is the amount of pollutant adsorbed (mg g^{-1}) at equilibrium, and k_1 (min^{-1}) is the rate constant of the adsorption process. The rate constant k_1 is detected from the slope of the straight line obtained from plotting $\log(q_e - q_t)$ versus t .

Pseudo-second-order model

The pseudo-second-order equation is expressed as:

$$\frac{t}{q_t} = \frac{1}{k_2 q_e^2} + \frac{1}{k_2 q_e^2} t \quad (4)$$

where q_t and q_e are the same as in the previous model and k_2 is the pseudo-second-order rate constant of the adsorption ($\text{g mg}^{-1} \text{min}^{-1}$). Plotting t/q_t versus t produces a straight line with intercept = the rate constant (k_2) and slope = $1/q_e$.

The parameters obtained from both models are presented in Table 1. As shown, the experimental results fit well the pseudo-second-order model where the correlation coefficients (R^2) values were close to unity. Also, the theoretical q_e values detected from the pseudo-second-order model were very close to the experimental results. On the other hand, analyzing the experimental results using the pseudo-first-order model gives lower values for the correlation coefficient (R^2) and very low values for q_e compared to the experimental values. These results indicate that the adsorption process follows the pseudo-second-order model, where the adsorption of Ni (II) ions occurs on an energetically heterogeneous surface. The rate constant (k_2) values detected from pseudo second-order model indicate that the rate of adsorption on gSt/Fe₃O₄/GO was slightly greater than that on gSt. This is attributed to the presence of GO sheets as well as Fe₃O₄ nanoparticles which enhances the adsorption.

Table 1 Kinetics parameters for the adsorption of Ni (II) ions (20 mg g^{-1}), pH 5, 20° C for 24 h

Adsorbent	q_e [experimental] (mg g^{-1})	Pseudo-first-order			Pseudo-second-order		
		q_e (mg g^{-1})	$K_1 \times 10^3$ (min^{-1})	R^2	q_e (mg g^{-1})	k_2 ($\text{g mg}^{-1} \text{min}^{-1}$)	R^2
gSt	9.028	1.528	5.093	0.908	9.175	34.017	0.999
gSt/Fe ₃ O ₄ /GO	9.500	1.446	2.650	0.811	9.615	37.846	0.999

Adsorption mechanism

The experimental adsorption data were examined using the intra-particle diffusion model to predict the adsorption mechanism and the rate determining step. This model assumes that the intra-particle diffusion process is the rate determining step and its rate can be detected using the following expression [33]:

$$q_t = k_i t^{1/2} + C \quad (5)$$

where k_i is the rate constant of intra-particle diffusion ($\text{mg g}^{-1} \text{min}^{-1/2}$) and C (mg g^{-1}) is an indicator for the boundary layer thickness and as the boundary layer effect increases, the value of C increases. According to this model, if plotting q_t versus the square root of time ($t^{1/2}$) yields a straight line passes through the origin then the intra-particle diffusion is the rate determining step. If the straight line deviates from the origin, then the intra-particle diffusion is not the only rate determining step. On the other hand, if the plot showed two or more overlapping lines, then two or more stages are controlling the adsorption process [22]. Figure 9 shows the intra-particle diffusion plot obtained from the experimental adsorption results. The plot showed three regions with three overlapping lines which indicate a three stages adsorption process with decreasing rates over the whole time range. The first region represents the fast surface adsorption stage where the Ni (II) ions diffuse from the solution to the surface of the adsorbent and this step is not a rate limiting step. The second region represents the slower intra-particle diffusion stage at which Ni (II) ions diffuse through the bulk of the adsorbent. The third region represents the equilibrium stage where the

rate of diffusion process slows down as a result of the low Ni (II) ions concentration in the solution or/and the saturation of the adsorbent surface. These observations suggest a multistep adsorption process where the intra-particle diffusion step is not the only rate determining stage but it influences the adsorption rate [9].

The intra-particle diffusion rate constant k_i is determined from the slope of the line that passes through the points of the second region in the plot and is listed in Table 2. As shown gSt/ Fe_3O_4 / GO exhibited lower value for k_i indicating slower intra-particle diffusion. Besides, according to obtained C values, the boundary layer thickness is greater in the case of gSt/ Fe_3O_4 / GO sample. This was attributed to the presence of the GO sheets and Fe_3O_4 impregnated in the polymeric matrix which may limit the rate of the diffusion process.

Adsorption isotherms

The adsorption equilibrium results attained after 24 h have been analyzed using Langmuir, Freundlich and Dubinin–Radushkevich (D-R) isotherm models. At these experiments, 0.1 g adsorbent was added to 50 ml Ni (II) ions solution with different initial concentrations range from

Table 2 Intra-particle diffusion parameters for Ni (II) ions adsorption

Adsorbent	Intraparticle diffusion mod		R^2
	k_i ($\text{mg g}^{-1} \text{min}^{-1/2}$)	C (mg g^{-1})	
gSt	0.1981	5.1257	0.927
gSt/ Fe_3O_4 / GO	0.0735	7.5729	0.968

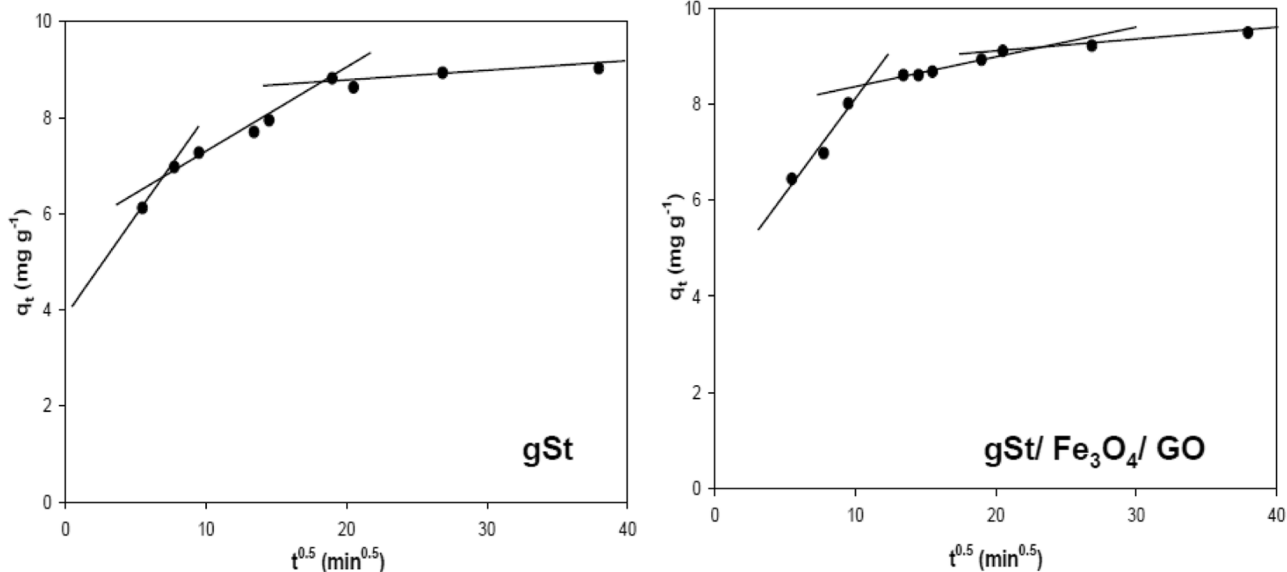


Fig. 9 Intra-particle diffusion plots for adsorption of Ni (II) ions, 20 mg L^{-1} at pH 5.0 and 20°C for 24 h

20 to 500 mg L⁻¹ at pH 5 and 20 °C with continuous shaking for 24 h.

Langmuir isotherm

This model suggests a monolayer adsorption where the active sites on the adsorbent have similar activation energy and affinity to the adsorbate. This model ignores the steric restrictions between the adjacent adsorbate species. Chemisorption process usually fits the linear mode of Langmuir isotherm model which is represented as [34]:

$$\frac{C_e}{q_e} = \frac{1}{bQ_e} + \frac{C_e}{q_e} \quad (6)$$

$$R_L = \frac{1}{1 + bC_e} \quad (7)$$

where C_e and q_e are the equilibrium concentration of adsorbed species in aqueous solution (mg L⁻¹) and on adsorbent (mg g⁻¹) respectively. Q_e is the theoretical capacity in the case of complete monolayer coverage (mg g⁻¹) and b is the Langmuir constant and it is correlated to the adsorption energy (L mg⁻¹). The dimensionless Langmuir factor R_L could be detected using Eq. 7 where C_0 is the maximum initial concentration of Ni(II) ions (mg L⁻¹). The numerical value for R_L indicates whether the adsorption is favorable ($R_L < 1$) or unfavorable ($R_L > 1$).

Freundlich isotherm

The Freundlich adsorption isotherm assumes a multilayer adsorption mechanism on the adsorbent which has several active sites with different adsorption energies. It suggests that the adsorbent has a heterogeneous surface with non-uniform distribution of adsorption heat instead of exponential decrease during the adsorption process [35]. The linear form of this model is represented as [36]:

$$\log q_e = \log k_f + \frac{1}{n} \log C_e \quad (8)$$

where q_e and C_e are similar to that in Langmuir model, k_f is the Freundlich constant is an indicator for the extent of

adsorption or adsorption capacity [mg g⁻¹ (mg L⁻¹)ⁿ] and $1/n$ is an empirical parameter related to the energetic heterogeneity of the adsorption sites (dimensionless). The constants k_f and $1/n$ can be detected from the intercept and the slope of $\log(q_e)$ versus $\log(C_e)$ plot. $1/n$ value lies between zero and 1 and the closer the value to zero the more heterogeneous surface is [9].

Dubinin–Radushkevich Isotherm

Dubinin–Radushkevich (D-R) isotherm is usually used to investigate the type of adsorption either physical or chemical in nature through the detection of the apparent free energy of adsorption. In general, this model is suitable for the adsorption processes that occur on heterogeneous surfaces with a Gaussian energy distribution. The linearized expression of this model is written as:

$$\ln q_e = \ln q_{(D-R)} - \beta \epsilon^2 \quad (9)$$

$$\epsilon = RT \ln\left(1 + \frac{1}{C_e}\right) \quad (10)$$

$$E = \frac{1}{\sqrt{2}} \quad (11)$$

where q_e and C_e are similar to that in Langmuir model, $q_{(D-R)}$ is the theoretical adsorption capacity (mg g⁻¹), ϵ is Polanyi potential and β is a constant related to the mean free energy of adsorption per one mole of the adsorbate (mol² kJ⁻²). R is the universal gas constant (0.008314 kJ K⁻¹ mol⁻¹) and T is the absolute temperature of adsorption experiment (K). E (kJ mol⁻¹) is the mean free energy per molecule of adsorbate when it migrates from the bulk of the solution (infinity) to the adsorbent surface and its numerical value suggests the nature of adsorption process. If E value ranges from 8 and 16 kJ mol⁻¹ then it is a chemisorption process while E value less than 8 kJ mol⁻¹ indicates that the adsorption is physisorption process [9].

The resulted parameters from fitting the experimental adsorption data with the three models are summarized in Table 3. Up to 200 mg l⁻¹ of Ni (II) ions solution initial

Table 3 Langmuir, Freundlich and Dubinin–Radushkevich (D-R) isotherms parameters

Adsorbent	Langmuir mode		R ²	Freundlich model			D-R isotherm		
	b (L mg ⁻¹)	q _{max} (mg g ⁻¹)		K _f (mg g ⁻¹)/ (mg L ⁻¹) ⁿ	1/n	R ²	E (kJ·mol ⁻¹)	QD-R (mg·g ⁻¹)	R ²
gSt	0.014	299.034	0.763	2.304	0.710	0.982	0.605	46.872	0.905
gSt/ Fe ₃ O ₄ / GO	0.020	417.104	0.537	3.208	0.636	0.976	>1.435	>49.393	0.906

concentration, both Freundlich and Langmuir models fit the experimental data and exhibit comparable R^2 values ($R^2 > 0.96$). This is attributed to the high adsorption capacity of the adsorbent and the low concentration of the adsorbate which results in both isotherm equations approach a linear form. Additional isotherm with initial concentration of 500 mg L^{-1} of Ni (II) ions is carried out to explore the best-fitted model and the results well fitted Freundlich model. The values of $1/n$ confirmed the heterogeneous nature of the surface where it was closer to zero in the case of gSt/ Fe_3O_4 / GO which suggests that this sample has a more heterogeneous surface than gSt. This is attributed to the decoration of the polymeric matrix by the inorganic nanoparticles. gSt/ Fe_3O_4 / GO showed higher k_f value than gSt, which reflects that gSt/ Fe_3O_4 / GO has a higher adsorption capacity.

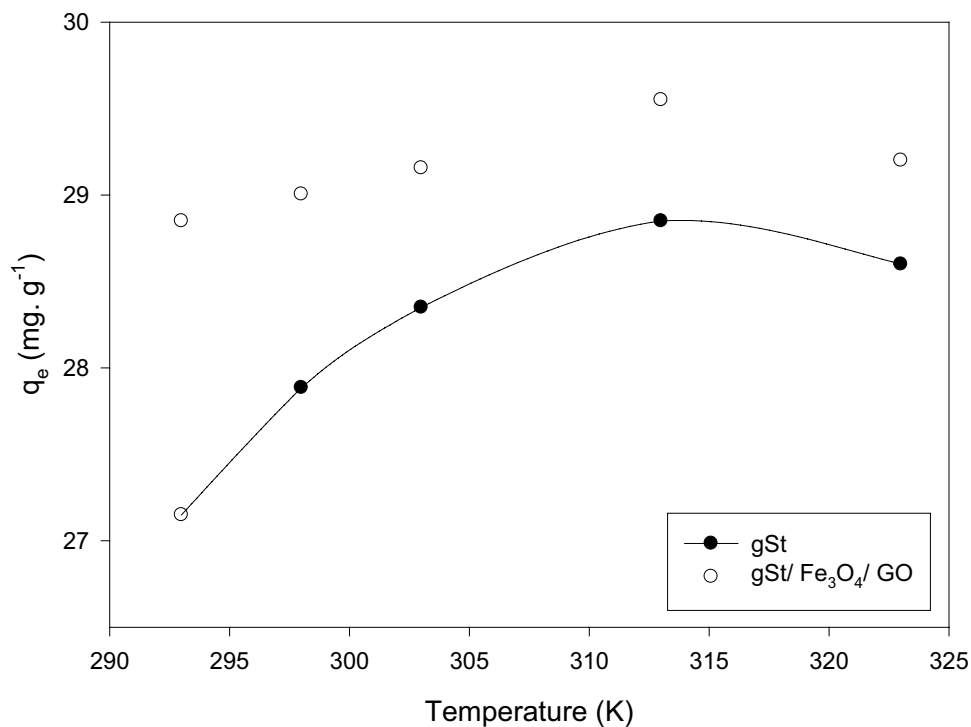
Dubinin-Radushkevich isotherm is restricted for a definite range of adsorbate concentrations where it shows unrealistic behavior at high concentrations and it is unable to predict Henry's law at low pressure [37]. Dubinin-Radushkevich isotherm fitted reasonably the experimental data in concentration range $20\text{--}150 \text{ mg L}^{-1}$ ($R^2 = 0.905$ and 0.906 for gSt and gSt/ Fe_3O_4 / GO, respectively). Both samples showed E value $< 8 \text{ kJ mol}^{-1}$ which suggests that the adsorption is physical in nature.

Thermodynamics studies

For the detection of thermodynamic parameters, 0.1 g of each adsorbent was immersed in 50 ml of Ni (II) aqueous

solution of initial concentration 60 mg L^{-1} at different temperatures (293, 298, 303, 313 and 323) for 24 h. Figure 10 shows that the adsorption capacity increases as temperature increase up to 313 K then dramatically decreased. These observations suggest that the adsorption process is endothermic in nature. As temperature increases, Ni(II) ions gain the required energy to diffuse through the polymeric adsorbent. Besides, increasing temperature allow the mobility of the polymeric chains which eases the diffusion of Ni(II) ions into the polymeric matrix. However, when the temperature exceeds 313 K, the adsorption capacity decreased which revealed to the low stability of the polymeric matrix at these temperatures. Generally, starch starts dissolution in aqueous medium at $40 \text{ }^\circ\text{C}$. Modification of the polymer by crosslinking would enhance the stability so the synthesized did not show dissolution at $40 \text{ }^\circ\text{C}$. However, it was reported that modification of starch by grafting may results in partial degradation of the chains into shorter fragments that leach out when soaking in solutions [38]. These results indicate that the synthesized samples are suitable as an adsorbent for aqueous solutions only up to $40 \text{ }^\circ\text{C}$. It is important to explore the thermodynamic parameters as entropy change (ΔS), enthalpy change (ΔH), and Gibbs energy change (ΔG) for the adsorption process. These parameters are calculated from the thermodynamic distribution coefficient (K_d) as follows:

Fig. 10 Effect of temperature on adsorption capacity for initial Ni (II) concentration 60 mg L^{-1} at pH 5.0 for 24 h



$$K_d = \frac{A_q}{A_c} = \frac{y_q q_e}{y_c C_e} \quad (12)$$

where A_q and A_c are the activity of the adsorbed Ni(II) ions and the activity of Ni(II) ions in the solution at equilibrium respectively. Y_q and y_c are the activity coefficients of adsorbed Ni (II) ions and the Ni(II) ions in solution at equilibrium. In the case of very dilute solutions of Ni (II) ions, the activity coefficients approach unity so the equation can be written as:

$$K_d = \frac{q_e}{C_e} \quad (13)$$

Then the thermodynamic parameters were detected as follows:

$$\Delta G = -RT \ln K_d \quad (14)$$

$$\ln K_d = \frac{\Delta S}{R} - \frac{\Delta H}{RT} \quad (15)$$

where T is the absolute temperature in Kelvin and R is the general gas constant ($8.314 \text{ J K}^{-1} \text{ mol}^{-1}$). ΔG is

calculated from Eq. 14 while ΔS and ΔH are detected from the intercept and the slope of the straight line obtained from plotting $\ln K_d$ versus $1/T$ up to 313 K. The detected thermodynamic parameters were listed in Table 4. The correlation coefficient R^2 values for the plot of $\ln K_d$ versus $1/T$ was 0.986 and 0.956 for gSt and gSt/ Fe_3O_4 / GO respectively so the calculated ΔH and ΔS values were satisfying. As shown in Table 4, the positive values of ΔH confirmed the endothermic nature of the adsorption process. Also, ΔS for both samples showed positive values indicating that the adsorption process results in more randomness, which confirmed that the adsorption of Ni(II) ions on the samples is favorable [22]. The negative values of ΔG up to 313 K suggest that the adsorption is spontaneous in nature. Also, increasing the temperature from 293 to 313 K resulted in more negative ΔG values for all samples which indicates that the adsorption is more spontaneous at a higher temperature. The less negative ΔG values at 323 K are misleading because at this temperature the dissolution of starch from the polymer takes place. These results revealed that increasing the temperature promotes the adsorption process up to 313 K.

Table 4 Thermodynamic parameters for adsorption of Ni(II) ions on synthesized samples

T (K)	gSt				gSt/ Fe_3O_4 / GO			
	$\ln K_d$	ΔG (J mol ⁻¹)	$\Delta H \times 10^3$ (J mol ⁻¹)	ΔS (J mol ⁻¹ K ⁻¹)	$\ln K_d$	ΔG (J mol ⁻¹)	$\Delta H \times 10^3$ (J mol ⁻¹)	ΔS (J mol ⁻¹ K ⁻¹)
293	1.5609	-3802.3820	1.8743	137.4929	2.5292	-6161.1384	1.8135	144.9757
298	1.8859	-4672.4206			2.6793	-6638.2419		
303	2.1507	-5417.9302			2.8485	-7175.7935		
313	2.5292	-6581.6939			3.4914	-9085.7226		

Table 5 Comparison of the maximum adsorption capacity (q_{\max}) at equilibrium of prepared gSt and gSt/ Fe_3O_4 / GO with previous adsorbents for Ni(II) ions

Adsorbent	q_{\max} (mg/g)	pH	Reference
gSt	195	5	Present study
gSt/ Fe_3O_4 / GO	290	5	Present study
kaolinite clay	166.67	6	[39]
graft copolymers of maltodextrin and chitosan with 2-acrylamido-2-methyl-1-propanesulfonic acid	32.74	8	[40]
Peat	61.27	5	[41]
Corn cob ash	107.4	6	[42]
Magnetite/Graphene Oxide/Chitosan Nanocomposite	12.24	7	[43]
Aminopyridine modified poly(styrene-alt maleic anhydride) crosslinked by 1,2-diaminoethane	76.92	5	[44]
Cellulose acetate/zeolite composite fiber	16.95	5.5	[45]
Polymeric adsorbent form the reaction of diethylenetriamine (DETA) or pentaethylenhexamine (PEHA) with 1,3,5-tris(6-isocyanatoethyl)-1,3,5-triazinane-2,4,6-trione	26.43	6	[46]
poly[N-(4-[4-(aminophenyl)methylphenylmethacrylamide])]	2.25	6	[47]
2-Acrylamido-2-methyl-1-propanesulfonic acid	20.30	7	[48]
Lignocellulose/montmorillonite nanocomposite	94.86	6.8	[49]

Comparison with previous studies

To emphasize the efficiency of the prepared adsorbents, the obtained maximum adsorption capacities of Ni(II) ions were compared with previous studies. Table 5 shows that gSt/Fe₃O₄/GO exhibited high adsorption capacity of Ni(II) ions compared with natural and synthetic polymer nanocomposites from previous studies. Accordingly, the prepared gSt/Fe₃O₄/GO nanocomposite could successfully be used for the removal of Ni(II).

Conclusions

The utilization of starch as a low-cost biodegradable adsorbent for the removal of heavy metals from industrial wastewater is a promising approach. Incorporation of magnetite nanoparticles and GO nanosheets into the polymeric matrix enhances the removal efficiency of heavy metals. In this study, starch-g-polyacrylamide and its nanocomposites with Fe₃O₄ nanoparticles and GO have been successfully synthesized and used as adsorbents for Ni (II) ions. The adsorption kinetics fitted the pseudo-second-order model. The equilibrium adsorption results were well described by Freundlich model and Dubinin – Radushkevich isotherms indicating a multilayer coverage of Ni (II) ions on the adsorbent surface through a physisorption mechanism. The adsorption occurs in three steps that starts with surface adsorption followed by intra-particle diffusion and finally equilibrium. The thermodynamic analysis showed that the adsorption is endothermic, spontaneous and leads to more disorder. The synthesized samples showed removal (%) of Ni(II) ions from aqueous solutions up to 90 and 95% on gSt and gSt/Fe₃O₄/GO respectively. These results suggested that gSt/Fe₃O₄/GO is a powerful adsorbent for Ni (II) ions from aqueous solutions.

Acknowledgements The authors are grateful to Prof. Soad Ashry, the professor at the national research center for the Atomic Absorption facilities. The authors also thank, Professor Mohamed Rashad, the Central Metallurgical Research and Development Institute for the VSM measurements.

References

- Jain M, Kumar Garg V, Kadirvelu K (2013) Removal of Ni(II) from aqueous system by chemically modified sunflower biomass. *Desalin Water Treat* 52:5681–5695
- Nirav PR, Prapti US, Nisha KS (2016) Adsorptive removal of nickel (II) ions from aqueous environment: A review. *J Environ Manag* 179:1–20
- Jong-Hwan P, Yong SO, Seong-Heon K, Ju-Sik Ch, Jong-Soo H, Ronald DD, Dong-Cheol S (2016) Competitive adsorption of heavy metals onto sesame straw biochar in aqueous solutions. *Chemosphere* 142:77–83
- Zafar MN, Aslam I, Nadeem R, Munir S, Rana UA, Khan SU-D (2015) Characterization of chemically modified biosorbents from rice bran for biosorption of Ni(II). *J Taiwan Inst Chem Eng* 46:82–88
- Keranen A, Leivisk T, Salakka A, Tanskanen J (2015) Removal of nickel and vanadium from ammoniacal industrial wastewater by ion exchange and adsorption on activated carbon. *Desalin Water Treat* 53:2645–2654
- Lalsing PK (2019) Rapid removal of nickel (II) by coconut leaves powder as bioadsorbent. *J Adv Chem Sci* 5:632–636
- Dhanashree C, Vikesh G, Virendra K (2014) Adsorptive removal of copper(II) from aqueous solution onto the waste sweet lime peels (SLP): equilibrium, kinetics and thermodynamics studies. *J Desalin Water Treat* 52:7822–7837
- Wu F-C, Tseng R-L, Juang R-S (2010) A review and experimental verification of using chitosan and its derivatives as adsorbents for selected heavy metals. *J Environ Manage* 91:798–806
- Ali O, Mohamed SK (2017) Adsorption of copper ions and alizarin red S from aqueous solutions onto a polymeric nanocomposite in single and binary systems. *Turkish J Chem* 41:967–986
- Abou El-Reash YG, Abdelghany AM, Lepold K (2017) Solid phase extraction of Cu²⁺ and Pb²⁺ from water using new thermally treated Chitosan/ Polyacrylamide thin films; Adsorption kinetics and thermodynamics. *Int J Environ Ana Chem* 97:965–982
- Esmat M, Farghali AA, Khedr MH, El-Sherbiny IM (2017) Alginate-Based Nanocomposites for Efficient Removal of Heavy Metal Ions. *Int J Bio Macromol* 102:272–283
- Niu HY, Pu LM, Li J (2015) Removal of Cu (II) Ions by a novel starch-based adsorbent from aqueous solution. *App Mechanics Mat* 713:2815–2818
- Ibrahim BM, Fakhre NA (2019) Crown ether modification of starch for adsorption of heavy metals from synthetic wastewater. *Int J Biolog Macromolecules* 123:70–80
- Naushad M, Ahamad T, Sharma G, Ala'a H, Albadarin AB, Alam MM, Alothman ZA, Alshehri SM, Ghfar AA (2016) Synthesis and characterization of a new starch/SnO₂ nanocomposite for efficient adsorption of toxic Hg²⁺ metal ion. *Chem Eng J* 300:306–316
- Hayeeye F, Yu QJ, Sattar M, Chinpa W, Sirichote O (2018) Adsorption of Pb²⁺ ions from aqueous solutions by gelatin/activated carbon composite bead form. *Adsorp Sci Techn* 36:355–371
- Baseri H, Tizro S (2017) Treatment of nickel ions from contaminated water by magnetite based nanocomposite adsorbents: Effects of thermodynamic and kinetic parameters and modeling with Langmuir and Freundlich isotherms. *Pro Safety Env Pro* 109:465–477
- Ekebafé LO, Ogbeifun DE, Okieimen FE (2012) Removal of heavy metals from aqueous media using native cassava starch hydrogel. *African J Env Sci Techn* 6:275–282
- Feng K, Wen G (2017) Adsorbed Pb²⁺ and Cd²⁺ ions in water by cross-linked starch xanthate. *Int J Polym Sci*. <https://doi.org/10.1155/2017/6470306>
- Sancey B, Trunfio GA, Crini G (2011) Heavy metal removal from industrial effluents by sorption on cross-linked starch: chemical study and impact on water toxicity. *J Env manag* 92:765–772
- Abdul-Raheim ARM, El-Saeed SM, Farag RK, Abdel-Raouf ME (2016) Low cost biosorbents based on modified starch iron oxide nanocomposites for selective removal of some heavy metals from aqueous solutions. *Adv Mater Lett* 7(5):402–409
- Massart R (1981) Preparation of aqueous magnetic liquids in alkaline and acidic media. *IEEE Trans Magn* 17:1247–1248
- Mohamed SK, Hegazy SH, Abdelwahab NA, Ramadan AM (2018) Coupled adsorption-photocatalytic degradation of crystal violet under sunlight using chemically synthesized grafted sodium alginate/ZnO/graphene oxide composite. *Int J Bio Macromol* 108:1185–1198

23. Hariani PL, Faizal M, Marsi R, Setiabudidaya D (2013) Synthesis and properties of Fe₃O₄ nanoparticles by co-precipitation method to removal procion dye. *Int J Env Sci Develop* 4:336–340
24. Kassae MZ, Motamedi E, Majdi M (2011) Magnetic Fe₃O₄-graphene oxide/polystyrene: Fabrication and characterization of a promising nanocomposite. *Chem Eng J* 172:540–549
25. Cheng X, Kumar V, Yokozeki T, Goto T, Takahashi T, Koyanagi J, Wu L, Wang R (2016) Highly conductive graphene oxide/polyaniline hybrid polymer nanocomposites with simultaneously improved mechanical properties. *Composites A* 82:100–107
26. Wang S, Zhang C, Chang Q (2017) Synthesis of magnetic crosslinked starch-graft-poly(acrylamide)-co-sodium xanthate and its application in removing heavy metal ions. *J Exp Nanosci* 12:270–284
27. Hosseinzadeh H, Ramin S (2015) Magnetic and pH-responsive starch-g-poly(acrylic acid-coacrylamide)/ graphene oxide superabsorbent nanocomposites: one-pot synthesis, characterization and swelling behavior. *Starch* 68:200–212
28. Rattana T, Chaiyakun S, Witit-anun N, Nuntawong N, Chindaudom P, Oaew S, Kedkeaw C, Limsuwan P (2012) Preparation and characterization of graphene oxide Nanosheets. *Procedia Eng* 32:759–764
29. Hoogmoed CG, Busscher HJ, Vos P (2003) Fourier transform infrared spectroscopy studies of alginate–PLL capsules with varying compositions. *J Biomed mat res* 67A:172–178
30. Zubir NA, Yacou C, Motuzas J, Zhang X, da Costa JCD (2014) Structural and Functional Investigation of Graphene Oxide-Fe₃O₄ nanocomposites for the Heterogeneous Fenton-Like Reaction. *Sci Rep* 4:4594–4601
31. Soleymani M, Akbari A, Mahdavinia GR (2018) Magnetic PVA/laponite RD hydrogel nanocomposites for adsorption of model protein BSA. *Polym Bull* 76:2321–2340
32. Wu L, Ye Y, Liu F, Tan C, Liu H, Wang S, Wang J, Yi W, Wu W (2013) Organo-bentonite-Fe₃O₄ poly(sodium acrylate) magnetic superabsorbent nanocomposite: Synthesis, characterization, and Thorium(IV) adsorption. *Appl Clay Sci* 83:405–414
33. Mohamed SK, Alazhary AM, Al-Zaqri N, Alsalmeh A, Alharthi FA, Hamdy MS (2020) Cost-effective adsorbent from arabinogalactan and pectin of cactus pear peels: Kinetics and thermodynamics studies. *Int J Biolog Macromol* 150:941–947
34. Dabrowski A (2001) Adsorption—From Theory to Practice. *Adv Colloid Interface Sci* 93:135–224
35. Adamson AW, Gast AP (1997) *Physical Chemistry of Surfaces*, sixth ed., Wiley– Interscience, New York
36. Freundlich H (1906) Ueber die adsorption in loesungen. *Zeitschrift für Physikalische Chemie* 57:385–470
37. Ayawei N, Ebelegi AN, Wankasi D (2017) Modelling and Interpretation of Adsorption Isotherms. *J Chem.* <https://doi.org/10.1155/2017/3039817>
38. Simi CK, Abraham TE (2007) Hydrophobic grafted and crosslinked starch nanoparticles for drug delivery. *Bioprocess Biosyst Eng* 30:173–180
39. Dawodu F, Akpomie K (2014) Simultaneous adsorption of Ni(II) and Mn(II) ions from aqueous solution unto a Nigerian kaolinite clay. *J Mater Res Tech* 3:129–141
40. Abdelrahman EA, Abdel-Salam ET, El Rayes SM, Mohamed NS (2019) Facile synthesis of graft copolymers of maltodextrin and chitosan with 2-acrylamido-2-methyl-1-propanesulfonic acid for efficient removal of Ni(II), Fe(III), and Cd(II) ions from aqueous media. *J Polym Res.* <https://doi.org/10.1007/s10965-019-1920-4>
41. Bartczak P, Norman M, Klapiszewski L, Karwanska N, Kawalec M, Baczynska M, Wysokowski M, Zdzarta J, Ciesielczyk F, Jesionowski T (2018) Removal of nickel(II) and lead(II) ions from aqueous solution using peat as a low-cost adsorbent: A kinetic and equilibrium study. *Arabian J Chem* 11:1209–1222
42. Singh H, Rattan V (2011) Adsorption of nickel from aqueous solutions using low cost biowaste adsorbents. *Water Quality Res J Canada* 46:239–249
43. Luyen TT, Hoang VT, Thu DL, Giang LB, Lam DT (2019) Studying Ni(II) adsorption of magnetite/graphene oxide/chitosan nanocomposite. *Adv polym tech.* <https://doi.org/10.1155/2019/8124351>
44. Samadi N, Hasanzadeh R, Rasad M (2015) Adsorption isotherms, kinetic, and desorption studies on removal of toxic metal ions from aqueous solutions by polymeric adsorbent. *J Appl Polym Sci* 132:41642
45. Ji F, Li C, Tang B, Xu J, Lu G, Liu P (2012) Preparation of cellulose acetate/zeolite composite fiber and its adsorption behavior for heavy metal ions in aqueous solution. *Chem Eng J* 209:325–333
46. Ceglowska M, Gierczyka B, Frankowska M, Popenda L (2018) A new low-cost polymeric adsorbents with polyamine chelating groups for efficient removal of heavy metal ions from water solutions. *Reac Func Polym* 131:64–74
47. Kushwaha AK, Gupta N, Chattopadhyaya MC (2017) Dynamics of adsorption of Ni(II) Co(II) and Cu(II) from aqueous solution onto newly synthesized poly[N-(4-[4-(aminophenyl)methylphenylmethacrylamide])]. *Arabian J Chem* 10:S1645–S1653
48. He H, Feng Q (2017) Preparation and application of Ni(II) ion-imprinted silica gel polymer for selective separation of Ni(II) from aqueous solution. *Roy soc chem* 7:15102–15111
49. Zhang X, Wang X (2015) Adsorption and Desorption of Nickel(II) Ions from Aqueous Solution by a Lignocellulose/Montmorillonite Nanocomposite. *PLoS ONE* 10:e0117077

Publisher's Note Springer Nature remains neutral with regard to jurisdictional claims in published maps and institutional affiliations.